Available online at www.sciencedirect.com
ScienceDirect
Journal of Solid State Chemistry 180 (2007) 1686–1697
JOURNAL OF SOLID STATE CHEMISTRY
www.elsevier.com/locate/jssc

# Hydrothermal synthesis, thermal, structural, spectroscopic and magnetic studies of the $Mn_{5-x}Co_x(HPO_4)_2(PO_4)_2(H_2O)_4$ ($x = 1.25$, 2, 2.5 and 3) finite solid solution

Edurne S. Larrea[a], José L. Mesa[a,*], José L. Pizarro[b], María I. Arriortua[b], Teófilo Rojo[a]

[a]*Departamento de Química Inorgánica, Facultad de Ciencia y Tecnología, Universidad del País Vasco/EHU, Apdo. 644, E-48080 Bilbao, Spain*
[b]*Departamento de Mineralogía y Petrología, Facultad de Ciencia y Tecnología, Universidad del País Vasco/EHU, Apdo. 644, E-48080 Bilbao, Spain*

Received 15 January 2007; received in revised form 9 March 2007; accepted 11 March 2007
Available online 19 March 2007

**Abstract**

The $Mn_{5-x}Co_x(HPO_4)_2(PO_4)_2(H_2O)_4$ ($x = 1.25$, 2, 2.5, 3) finite solid solution has been synthesized by mild hydrothermal conditions under autogeneous pressure. The phases crystallize in the $C2/c$ space group with $Z = 4$, belonging to the monoclinic system. The unit-cell parameters obtained from single crystal X-ray diffraction are: $a = 17.525(1)$, $b = 9.0535(6)$, $c = 9.4517(7)$ Å, $\beta = 96.633(5)$ ° being $R1 = 0.0436$, $wR2 = 0.0454$ for Mn75Co25; $a = 17.444(2)$, $b = 9.0093(9)$, $c = 9.400(1)$ Å, $\beta = 96.76(1)$ ° being $R1 = 0.0381$, $wR2 = 0.0490$ for Mn60Co40; $a = 17.433(2)$, $b = 8.9989(9)$, $c = 9.405(1)$ Å, $\beta = 96.662(9)$ ° being $R1 = 0.0438$, $wR2 = 0.0515$ for Mn50Co50 and $a = 17.4257(9)$, $b = 8.9869(5)$, $c = 9.3935(5)$ Å, $\beta = 96.685(4)$ ° being $R1 = 0.0296$, $wR2 = 0.0460$ for Mn40Co60. The structure consists of a three dimensional network formed by octahedral pentameric entities $(Mn,Co)_5O_{16}(H_2O)_6$ sharing vertices with the $(PO_4)^{3-}$ and $(HPO_4)^{2-}$ tetrahedra. The limit of thermal stability of these compounds is, approximately, 165 °C, near to this mean temperature the phases loose their water content in two successive steps. IR spectra show the characteristic bands of the water molecules and the phosphate and hydrogen-phosphate oxoanions. The diffuse reflectance spectra are consistent with the presence of $MO_6$ octahedra environments in slightly distorted octahedral geometry, except for the $M(3)O_6$ octahedron which presents a remarkable distortion and so a higher Dq parameter. The mean value for the Dq and B-Racah parameter for the $M(1),(2)O_6$ octahedra is 685 and 850 $cm^{-1}$, respectively. These parameters for the most distorted $M(3)O_6$ polyhedron are 825 and 880 $cm^{-1}$, respectively. The four phases exhibit antiferromagnetic couplings as the major magnetic interactions. However, a small spin canting phenomenon is observed at low temperatures for the two phases with major content in the anisotropic-Co(II) cation.
© 2007 Published by Elsevier Inc.

*Keywords:* Finite solid solution; Crystal structure; Thermal study; IR and UV–Vis; Magnetic properties

## 1. Introduction

Transition metal phosphates have received great interest in recent years. The great ability of the phosphate framework to stabilize different oxidation states is produced for the relatively high charge in $(PO_4)^{3-}$ tetrahedra that favors the formation of anionic frameworks with a high degree of mechanical, chemical and thermal stability [1,2]. These compounds, minerals in some cases, offer a considerable number of structures, which can give rise to original physical properties (magnetic, heterogeneous catalysis, ion exchange, optical, etc.) with potential applications. Hydrothermal techniques can be used as an adequate synthetic method to obtain minerals or complex phosphates with transition metals. A systematic variation of the temperature and pressure can originate interesting structural phases.

A large variety of manganese(II) and cobalt(II) phosphates is now known. The $M_5(OH)_4(PO_4)_2$ ($M$ = Mn and Co) compounds are isostructural between them and with the *arsenoclasite* mineral, $Mn_5(OH)_4(AsO_4)_2$ [3]. The crystal structure of these phases contains M(II) cations located on five different crystallographic positions with a

*Corresponding author. Fax: +34 94 601 35 00.
*E-mail address:* joseluis.mesa@ehu.es (J. L. Mesa).

0022-4596/$ - see front matter © 2007 Published by Elsevier Inc.
doi:10.1016/j.jssc.2007.03.012

chain structure. Other species with both metallic cations is the hydrated hydrogenphosphate $M(H_2PO_4)_2.2H_2O$ [4], which crystal structure is formed by layers containing $MO_6$ octahedra and $PO_4$ tetrahedra, extended in parallel stacking along the *c*-crystallographic axis. In this phase the sheets are linked by hydrogen bonds. Additionally, the $Mn_3(OH)_2(PO_4)_2(H_2O)$ *bermanite* mineral [5] exhibits a layered structure in which the sheets are linked by short chains formed by one $MnO_6$ octahedron and two $PO_4$ tetrahedra. The $Mn_3(PO_4)_2(H_2O)_7$, *switzerite*, and $Mn_3(PO_4)_2(H_2O)_4$, *metaswitzerite*, exhibit layered and three-dimensional structure, respectively [6]. The crystal structure of $Mn(PO_4)(H_2O)$, resolved by X-ray powder diffraction data, reveals a zig-zag chain of Mn(II) ions [7]. Two phases with $Co_3(PO_4)_2nH_2O$ composition are known for the cobalt(II) ion. One of them with one water molecule and the other one with eight water molecules. The latter is related to the $Fe_3(PO_4)_2(H_2O)_8$ *vivianite* mineral [8]. Although single-crystals suitable for X-ray diffraction study of these compounds were obtained, unfortunately, in several, cases pure phases have not been prepared. This fact has precluded carrying out any study on the physical properties of these materials. In this way, we have recently studied the $M_7(HPO_4)_4(PO_4)_2$ ($M$ = Mn and Co) phases [9] that present a complex three-dimensional network of Mn(II) or Co(II) ions with antiferromagnetic couplings.

The crystal structure of $Mn_5(HPO_4)_2(PO_4)_2(H_2O)_4$, isostructural with the *hureaulite* mineral, was determined by Gerault et al. from single-crystal X-ray diffraction data [10a]. The crystal structures of the isostructural $Mn_{5-x}Co_x(HPO_4)_2(PO_4)_2(H_2O)_4$ ($x = 1.25$, 2, 2.5, 3) finite solid solution are reported in this work. The structure consists of a three-dimensional framework built from $Mn_5O_{16}(H_2O)_6$ pentameric units formed by edge-sharing octahedra. The structure contains $MnO_6$ octahedra, $HPO_4$ and $PO_4$ tetrahedra. Along the c-axis the existence of channels occupied by the water molecules with their hydrogen atoms directed into the cavities can be underlined. The other isostructural extreme of the solid solution, $Co_5(HPO_4)_2(PO_4)_2(H_2O)_4$, based only on the Co(II) cation, has been recently reported by Han et al. [10b].

As a part of our general investigation about the crystal chemistry and physical behavior of phosphate compounds [11] we report the mild hydrothermal synthesis, crystal structure and the study of the thermal, spectroscopic and magnetic properties of the $Mn_{5-x}Co_x(HPO_4)_2(PO_4)_2(H_2O)_4$ ($x = 1.25$, 2, 2.5 and 3) finite solid solution, which exhibits predominant antiferromagnetic couplings and a phenomenon of weak ferromagnetism, at low temperature, for the components with major content in the anisotropic Co(II) cation. Furthermore, a comparative magnetic study, on the basis of the main magnetic parameters, for the four phases belonging to the finite solid solution is carried out, together with a qualitative analysis of the more important exchange and superexchange magnetic pathways in these phases.

## 2. Experimental section

### 2.1. Synthesis and characterization

The members of the $Mn_{5-x}Co_x(HPO_4)_2(PO_4)_2(H_2O)_4$ ($x = 1.25$, 2, 2.5 and 3) finite solid solution were synthesized using mild hydrothermal conditions under autogeneous pressure. Taking into account the percentage of the metallic cations, the phases will be named Mn75Co25, Mn60Co40, Mn50Co50 and Mn40Co60. The starting reagents were $MnCl_2 \cdot 4H_2O$ (112.5 mg, 0.57 mmol; 90.0 mg, 0.45 mmol; 75.0 mg, 0.38 mmol and 60.0 mg, 0.30 mmol for each composition, respectively) $CoCl_2 \cdot 6H_2O$ (45.0 mg 14.61 mmol; 72.0 mg, 0.30 mmol; 90.0 mg, 0.38 mmol and 108.0 mg, 0.45 mmol for each composition, respectively), $H_3PO_4$ (1 ml; 14.6 mmol in all cases) and triethylamine (2.0 ml; 14.20 mmol) up to a pH of 4. This reaction mixture was solved in 28 ml of water and then placed in a PTFE-lined stainless steel pressure vessel (fill factor 75%). Light pink single-crystals appeared after 5 days of reaction at 170 °C, without any change in the initial pH of the reaction. The yield being, approximately, 80%.

Attempts performed in order to obtain other phases with a Co(II)-percentage higher than 60% were unsuccessful. The chemical experiments were carried out regulating the pH at different values distinct of 4.0, using different organic diamines. Besides, the relative amounts of the reagents were also modified. However, all the synthetic experiments were unsuccessful. In all cases, a $Mn_{5-x}Co_x(HPO_4)_2(PO_4)_2(H_2O)_4$ member of the solid solution, with a Co(II) percentage near to 60%, is obtained, together with the $Co_3(HPO_4)_2(OH)_2$ phase [12]. These results suggest that the stability of $Co_3(HPO_4)_2(OH)_2$, in the nearest of a 60% of substitution of Mn(II) for Co(II) in the title solid solution, is higher than the stability of the $Mn_{5-x}Co_x(HPO_4)_2(PO_4)_2(H_2O)_4$ ($x = 3$) substituted member of the solid solution. This fact precludes, probably, to obtain new phases belonging to the solid solution, with a percentage of Co(II) cation higher than, approximately, 60%.

The percentage of the elements in the phases was measured by atomic absorption spectroscopy (AAS). Mn75Co25: Found: Mn, 27.9; Co, 9.5; required: Mn, 28.1; Co, 10.0. Mn60Co40: Found: Mn, 22.3; Co, 15.9; required: Mn, 22.4; Co, 16.0. Mn50Co50: Found: Mn, 18.5; Co, 19.7; required: Mn, 18.6; Co, 19.9. Mn40Co60: Found: Mn, 14.7; Co, 23.5; required: Mn, 14.8; Co, 23.9. The densities were measured by picnometry, the values being 3.26(1), 3.31(1), 3.34(1) and 3.35(1) $g\,cm^{-3}$ for Mn75Co25, Mn60Co40, Mn50Co50 and Mn40Co60, respectively. These values are near to those reported from the X-ray diffraction data, as can be seen in Table 1.

All phases have been characterized by X-ray powder diffraction data. The unit cell-parameters were obtained with the DICVOL program [13] and then refined with the pattern matching routine of the FULLPROF program [14], giving the following unit-cell parameters: $a = 17.541(1)$,

Table 1
Details of the crystal data, structural resolution and refinement procedure for $Mn_{5-x}Co_x(HPO_4)_2(PO_4)_2(H_2O)_4$ ($x = 1.25$, 2, 2.5 and 3)

| Formula | $Mn_{3.75}Co_{1..25}(HPO_4)_2$ | $Mn_3Co_2(HPO_4)_2$ | $Mn_{2.5}Co_{2.5}(HPO_4)_2$ | $Mn_2Co_3(HPO_4)_2$ |
|---|---|---|---|---|
| | $(PO_4)_2(H_2O)_4$ | $(PO_4)_2(H_2O)_4$ | $(PO_4)_2(H_2O)_4$ | $(PO_4)_2(H_2O)_4$ |
| Molecular weight ($g\,mol^{-1}$) | 733.65 | 736.64 | 738.64 | 740.63 |
| Crystalline system | Monoclinic | Monoclinic | Monoclinic | Monoclinic |
| Space group (No.) | *C*2/c (15) | *C*2/c (15) | *C*2/c (15) | *C*2/c (15) |
| a (Å) | 17.525(1) | 17.444(2) | 17.433(2) | 17.4257(9) |
| b (Å) | 9.0535(6) | 9.0093(9) | 8.9989(9) | 8.9869(5) |
| c (Å) | 9.4517(7) | 9.400(1) | 9.405(1) | 9.3935(5) |
| $\beta$ (º) | 96.633(5) | 96.76(1) | 96.662(9) | 96.685(4) |
| V ($Å^3$) | 1489.6(2) | 1467.0(3) | 1465.4(3) | 1461.0(1) |
| *Z* | 4 | 4 | 4 | 4 |
| $\rho_{calc}$ ($gr\,cm^{-3}$) | 3.271 | 3.335 | 3.348 | 3.367 |
| F(000) | 1430 | 1436 | 1440 | 1444 |
| *Collection data* | | | | |
| Temperature (K) | 293(2) | 293(2) | 293(2) | 293(2) |
| Diffractometer | Oxford Diffraction Xcalibur2 | Oxford Diffraction Xcalibur2 | Oxford Diffraction Xcalibur2 | Oxford Diffraction Xcalibur2 |
| μ ($mm^{-1}$) | 5.004 | 5.283 | 5.424 | 5.576 |
| Radiation, $\lambda$(MoKα) (Å) | 0.71073 | 0.71073 | 0.71073 | 0.71073 |
| Cristal size (mm) | $0.1 \times 0.05 \times 0.02$ | $0.16 \times 0.07 \times 0.01$ | $0.2 \times 0.04 \times 0.04$ | $0.09 \times 0.05 \times 0.01$ |
| Range $\theta$ (°) | 3.25–30.03 | 3.26–30.03 | 3.27–31.84 | 3.27–30.03 |
| Interval *h*, *k*, *l* | $\pm 24$, $\pm 12$, $-13 \leqslant l \leqslant 8$ | $\pm 24$, $\pm 12$, $-13 \leqslant l \leqslant 9$ | $-25 \leqslant h \leqslant 24$, $\pm 12$, $-10 \leqslant l \leqslant 13$ | $\pm 24$, $\pm 12$, $-13 \leqslant l \leqslant 11$ |
| No. of measured reflections | 7015 | 6949 | 7323 | 6898 |
| No. of independent reflections | 2137 | 2132 | 2332 | 2099 |
| *R* (int) | 0.0334 | 0.0350 | 0.0338 | 0.0313 |
| *Refinement* | | | | |
| Data/restrictions/parameter | 2137/6/155 | 2132/6/155 | 2332/1/155 | 2099/6/155 |
| *R* factors [$I > 2\sigma(I)$] | $R1 = 0.0237$, $wR2 = 0.0420$ | $R1 = 0.0242$, $wR2 = 0.0464$ | $R1 = 0.0256$, $wR2 = 0.0484$ | $R1 = 0.0212$, $wR2 = 0.0441$ |
| *R* factors [all data] | $R1 = 0.0436$, $wR2 = 0.0454$ | $R1 = 0.0381$, $wR2 = 0.0490$ | $R1 = 0.0438$, $wR2 = 0.0515$ | $R1 = 0.0296$, $wR2 = 0.0460$ |
| Máx. and Min. of electronic residual density ($e\,Å^{-3}$) | 0.562, −0.413 | 0.494, −0.453 | 0.669, −0.564 | 0.573, −0.444 |
| G. O. F | 0.928 | 0.926 | 0.921 | 0.961 |

$$R1 = \frac{\sum||F_o| - |F_c||}{\sum|F_o|}; \quad wR2 = \sqrt{\frac{\sum w(|F_o| - |F_c|)^2}{\sum w|F_o|^2}}$$

$w = 1/[\sigma^2|F_o|^2 + (xp)^2]$ with $p = [\max|F_o|^2 + 2|F_c|^2]/3$, where $x = 0.0181$, $x = 0.0237$, $x = 0.0230$, $x = 0.0248$

$b = 9.064(1)$, $c = 9.460(1)$ Å, $\beta = 96.66(1)^\circ$ for Mn75Co25 with $Rp = 6.38$, $Rwp = 8.70$, $\chi^2 = 1.38$; $a = 17.505(1)$, $b = 9.024(1)$, $c = 9.441(1)$ Å, $\beta = 96.70(1)^\circ$ for Mn60Co40 with $Rp = 7.10$, $Rwp = 9.61$, $\chi^2 = 1.63$; $a = 17.475(1)$, $b = 9.010(1)$, $c = 9.422(1)$ Å, $\beta = 96.66(1)^\circ$ for Mn50Co50 with with $Rp = 5.46$, $Rwp = 7.27$, $\chi^2 = 1.23$ and $a = 17.4397(1)$, $b = 8.999(1)$, $c = 9.407(1)$ Å, $\beta = 96.63(1)^\circ$ for Mn40Co60 with $Rp = 6.35$, $Rwp = 8.52$, $\chi^2 = 1.26$. These values are similar to those reported in the literature for the $M(HPO_4)_2(PO_4)_2(H_2O)_4$ ($M^{II}$ = Mn, Co) phases [10]. The diffraction peaks observed in the diffractograms of the finite solid solution members were indexed in the *C*2/*c* space group, confirming the chemical purity of all the components and the isostructural character with the $M(HPO_4)_2(PO_4)_2(H_2O)_4$ ($M^{II}$ = Mn, Co) compounds [10].

### 2.2. Thermal study

Thermogravimetric analyses were carried out under air in a DSC 2960 Simultaneous DSC-TGA TA Instrument. Crucibles containing ca. 20 mg of the samples were heated at 5 °C $min^{-1}$ in the temperature range 30–800 °C. Thermal elimination of the water molecules takes place in the 150–390 °C range, with two superimposed steps. The first step occurs in the 150–350 °C range and the mass loss can be associated with the elimination of one water molecule (mean exp. 1.5%, mean calc. 2.4%). The second one takes place in the 330–390 °C range and corresponds with the elimination of the three water molecules (mean exp. 8.9%, mean calc. 7.3%). The observed differences between the experimental and calculated mass loss can be associated to the partial overlapping of the two successive dehydration

steps. Finally, in the 390–530 °C temperature range a mean loss of 1.9% in mass occurs, which could be associated to the transformation of the hydrogen-phosphate anions, into the phosphate groups. The inorganic residues obtained at 800 °C were characterized by X-ray powder diffraction data and correspond to the $Mn_2(P_2O_7)$ [$C2/m$, $a = 6.636$, $b = 8.584$, $c = 4.5457$ Å, $\beta = 102.78$ °] [15a], $Co_2(P_2O_7)$ [$P2_1/c$, $a = 9.851$, $b = 8.359$, $c = 8.992$ Å, $\beta$ 133.57°] [15b] and the $(Mn,Co)_3(PO_4)_2$ isostructural with $Mn_3(PO_4)_2$ [$P2_1/c$, $a = 8.788$, $b = 11.434$, $c = 6.255$ Å, $b = 98.98$°] [15c]. The proposed decomposition reaction is

$$M_5(HPO_4)_2(PO_4)_2(H_2O)_4(s) \rightarrow M_2P_2O_7(s) + M_3(PO_4)_2(s) + 5H_2O(g)(M = Mn, Co).$$

The thermal behavior was also studied using time-resolved X-ray thermodiffractometry in air. A PHILIPS X'PERT automatic diffractometer (CuKα radiation) equipped with a variable temperature stage (Anton Paar HTK16) with a Pt sample holder was used in the experiment. The powder patterns were recordered in $2\theta$ steps of 0.06° in the range $5 \leqslant 2\theta \leqslant 40$ °, counting for 2 s per step and increasing the temperature at 5 °C min$^{-1}$ from room temperature up to 805 °C. The results for the Mn50Co50 member of the finite solid solution are illustrated in Fig. 1. From room temperature up to 355 °C a decrease of the intensity in the diffraction peaks when increasing temperature is observed. At around 355 °C the crystal structure collapses, probably due to the elimination of the water molecules, giving rise to two phases which are isostructural with the $Mn_2(P_2O_7)$ [$C2/m$, $a = 6.636$, $b = 8.584$, $c = 4.5457$ Å, $\beta = 102.78$°] [15a] and $Co_2(P_2O_7)$ [$P2_1/c$, $a = 8.851$, $b = 8.359$, $c = 8.992$ Å, $\beta = 133.57$°] [15b] that form the inorganic residue and are maintained up to 800 °C. Above 550 °C the diffraction peaks corresponding to the $(Mn,Co)_3(PO_4)_2$ isostructural with $Mn_3(PO_4)_2$ [$P2_1/c$, $a = 8.788$, $b = 11.434$, $c = 6.255$ Å, $\beta = 98.98$°] [15c] are also observed in the inorganic residue. The peaks of these residual phases increase when increasing temperature probably due to a better crystallization at high temperatures.

### 2.3. Single-crystal X-ray diffraction

Needle single-crystals with dimensions given in Table 1, were selected under a polarizing microscope and mounted on glass fibres. Single-crystal X-ray diffraction data were collected at room temperature on an Oxford Diffraction XCALIBUR2 automatic diffractometer (MoKα radiation) equipped with a CCD detector. Details of crystal data and some features of the structure refinement are reported in Table 1.

Data collection and Lorentz-Polarization and absorption corrections were made with the diffractometer software, taking into account the size and shape of the crystals [16]. The structures were solved by direct methods SHELXS97 [17] in the $C2/c$ space group, which allowed to obtain the positions of the Co(II), Mn(II) ions and phosphorous atoms. The refinement of the crystal structures was performed by full matrix least-squares based on $F^2$, using SHELXL97 program [18], obtaining the oxygen atoms. Scattering factors were taken from Ref. [19]. Anisotropic thermal parameters were refined for all atoms except the hydrogen ones, which were refined isotropically, with a constraint in the O–H bond lengths in the case of the water molecules. Nevertheless, the occupation of each metallic position has been refined, obtaining an unequal distribution of the metals in the three different crystallographic positions. The occupancy factors for Co(II) and Mn(II) cations in each compound were refined taking into account their stoichiometries and retraining to sum five atoms, according to the chemical formulas. Final $R$-factors

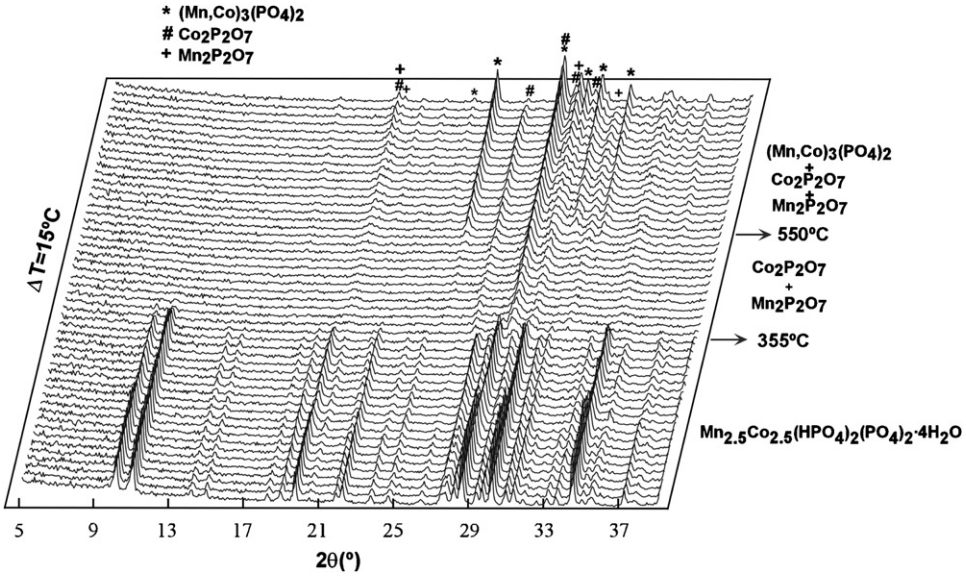


Fig. 1. Thermodiffractogram characteristic for the $Mn_{5-x}Co_x(HPO_4)_2(PO_4)_2 \cdot (H_2O)_4$ ($x = 1.25$, 2, 2.5, 3) phases.

are given in Table 1, together with the maximum and minimum peaks in the final Fourier differences synthesis and the goodness of the fits. Simulations based on the crystal structures of the four phases were in excellent agreement with the X-ray powder data, indicating the presence of pure compounds with high crystallinity. The structure drawings were made using the ATOMS program [20]. Atomic coordinates are given in Table 2. The rest of the tables, with selected bond distances and angles, for Mn75Co25, Mn60Co40, Mn50Co50 and Mn40Co60 are given as Supplementary Material in Tables S.M.1–4.

### 2.4. Physicochemical characterization techniques

The IR spectra (KBr pellets) were obtained with a Nicolet FT-IR 740 spectrophotometer in the 400–4000 $cm^{-1}$ range. Diffuse reflectance spectra were registered at room temperature on a Cary 5000 spectrophotometer in the 210–2000 nm range. Magnetic measurements on powdered samples were performed in the temperature range 2–300 K, using a Quantum Design MPMS-7 SQUID magnetometer. The magnetic field was 0.1 T, a value in the range of linear dependence of magnetization vs. magnetic field, even at 2.0 K.

## 3. Results and discussion

### 3.1. Crystal structure

The $Mn_{5-x}Co_x(HPO_4)_2(PO_4)_2(H_2O)_4$ ($x = 1.25$, 2, 2.5, 3) finite solid solution is isostructural with the *hureaulite* mineral with formula $(Mn,Fe)_5(HPO_4)_2(PO_4)_2(H_2O)_4$ [10]. The structure consists of a three dimensional network (Fig. 2), formed by octahedral pentameric entities $(Mn,Co)_5O_{16}(H_2O)_6$ sharing the O(5) and $O(9)_w$ edges with the ($PO_4$) and ($HPO_4$) tetrahedra (Fig. 3). This 3D network exhibits holes along the [001] direction with the hydrogen atoms of the water molecules pointing out towards these ones (see Fig. 2).

The mean metal–oxygen bond distances in the $[Mn,Co(1)O_6]$, $[Mn,Co(2)O_6]$ and $[Mn,Co(3)O_6]$ metallic octahedral polyhedral varies with the amount of cobalt(II)

Table 2
Atomic coordinates, equivalent temperature factors ($Å^2$), $U_{eq}$ and occupancy factors (O.F.) for $Mn_{5-x}Co_x(HPO_4)_2(PO_4)_2(H_2O)_4$ ($x = 1.25$, 2, 2.5, 3)

| Atom | Phase | x | y | z | $U_{eq}$ | O.F. |
|---|---|---|---|---|---|---|
| Mn(1)/Co(1) | Mn75C025 | 0 | 0.8966(1) | 0.25 | 9(1) | 0.44(1)/0.06(1) |
| | Mn60Co40 | 0 | 0.8968(1) | 0.25 | 10(1) | 0.33(1)/0.17(1) |
| | Mn50Co50 | 0 | 0.8971(1) | 0.25 | 9(1) | 0.30(1)/0.20(1) |
| | Mn40Co60 | 0 | 0.8975(1) | 0.25 | 9(1) | 0.25(1)/0.25(1) |
| Mn(2)/Co(2) | Mn75C025 | 0.1833(1) | 0.4129(1) | 0.3144(1) | 9(1) | 0.53(1)/0.47(1) |
| | Mn60Co40 | 0.1836(1) | 0.4132(1) | 0.3142(1) | 9(1) | 0.33(1)/0.67(1) |
| | Mn50Co50 | 0.1838(1) | 0.4134(1) | 0.3141(1) | 9(1) | 0.24(1)/0.76(1) |
| | Mn40Co60 | 0.1839(1) | 0.4136(1) | 0.3138(1) | 9(1) | 0.12(1)/0.88(1) |
| Mn(3)/Co(3) | Mn75C025 | 0.1747(1) | 0.0279(1) | 0.3653(1) | 10(1) | 0.90(1)/0.10(1) |
| | Mn60Co40 | 0.1748(1) | 0.0277(1) | 0.3655(1) | 10(1) | 0.83(1)/0.17(1) |
| | Mn50Co50 | 0.1748(1) | 0.0273(1) | 0.3658(1) | 10(1) | 0.71(1)/0.29(1) |
| | Mn40Co60 | 0.1748(1) | 0.0269(1) | 0.3662(1) | 9(1) | 0.63(1)/0.37(1) |
| P(1) | Mn75C025 | 0.0830(1) | 0.1805(1) | 0.0906(1) | 8(1) | 1 |
| | Mn60Co40 | 0.0830(1) | 0.1807(1) | 0.0907(1) | 7(1) | 1 |
| | Mn50Co50 | 0.0830(1) | 0.1805(1) | 0.0909(1) | 7(1) | 1 |
| | Mn40Co60 | 0.0829(1) | 0.1803(1) | 0.0910(1) | 7(1) | 1 |
| P(2) | Mn75C025 | 0.3387(1) | 0.2383(1) | 0.3729(1) | 7(1) | 1 |
| | Mn60Co40 | 0.3386(1) | 0.2382(1) | 0.3730(1) | 7(1) | 1 |
| | Mn50Co50 | 0.3385(1) | 0.2384(1) | 0.3728(1) | 7(1) | 1 |
| | Mn40Co60 | 0.3385(1) | 0.2386(1) | 0.3727(1) | 7(1) | 1 |
| O(1) | Mn75C025 | 0.0121(1) | 0.2857(2) | 0.0811(2) | 15(1) | 1 |
| | Mn60Co40 | 0.0120(1) | 0.2861(2) | 0.0810(2) | 15(1) | 1 |
| | Mn50Co50 | 0.0116(1) | 0.2859(2) | 0.0809(2) | 14(1) | 1 |
| | Mn40Co60 | 0.0113(1) | 0.2860(2) | 0.0806(2) | 14(1) | 1 |
| O(2) | Mn75C025 | 0.0767(1) | 0.0668(2) | 0.2064(2) | 12(1) | 1 |
| | Mn60Co40 | 0.0767(1) | 0.0664(2) | 0.2070(2) | 12(1) | 1 |
| | Mn50Co50 | 0.0769(1) | 0.0657(2) | 0.2071(2) | 12(1) | 1 |
| | Mn40Co60 | 0.0770(1) | 0.0657(2) | 0.2076(2) | 12(1) | 1 |
| O(3) | Mn75C025 | 0.1546(1) | 0.2730(2) | 0.1345(2) | 13(1) | 1 |
| | Mn60Co40 | 0.1549(1) | 0.2737(2) | 0.1354(2) | 12(1) | 1 |
| | Mn50Co50 | 0.1548(1) | 0.2741(2) | 0.1350(2) | 12(1) | 1 |

Table 2 (*continued*)

| Atom | Phase | *x* | *y* | z | $U_{eq}$ | O.F. |
|---|---|---|---|---|---|---|
| | Mn40Co60 | 0.1550(1) | 0.2741(2) | 0.1353(2) | 12(1) | 1 |
| O(4) | Mn75C025 | 0.4153(1) | 0.3905(2) | 0.0556(2) | 13(1) | 1 |
| | Mn60Co40 | 0.4153(1) | 0.3905(2) | 0.0556(2) | 12(1) | 1 |
| | Mn50Co50 | 0.4154(1) | 0.3904(2) | 0.0561(2) | 12(1) | 1 |
| | Mn40Co60 | 0.4154(1) | 0.3910(2) | 0.0561(2) | 12(1) | 1 |
| O(5) | Mn75C025 | 0.1641(1) | 0.2379(2) | 0.4654(2) | 11(1) | 1 |
| | Mn60Co40 | 0.1644(1) | 0.2380(2) | 0.4652(2) | 10(1) | 1 |
| | Mn50Co50 | 0.1644(1) | 0.2376(2) | 0.4651(2) | 10(1) | 1 |
| | Mn40Co60 | 0.1646(1) | 0.2373(2) | 0.4651(2) | 10(1) | 1 |
| O(6) | Mn75C025 | 0.2976(1) | 0.0939(2) | 0.3264(2) | 10(1) | 1 |
| | Mn60Co40 | 0.2973(1) | 0.0935(2) | 0.3261(2) | 10(1) | 1 |
| | Mn50Co50 | 0.2971(1) | 0.0938(2) | 0.3262(2) | 11(1) | 1 |
| | Mn40Co60 | 0.2971(1) | 0.0936(2) | 0.3258(2) | 11(1) | 1 |
| O(7) | Mn75C025 | 0.2975(1) | 0.3670(2) | 0.2900(2) | 11(1) | 1 |
| | Mn60Co40 | 0.2973(1) | 0.3673(2) | 0.2898(2) | 10(1) | 1 |
| | Mn50Co50 | 0.2969(1) | 0.3676(2) | 0.2891(2) | 11(1) | 1 |
| | Mn40Co60 | 0.2970(1) | 0.3678(2) | 0.2886(2) | 10(1) | 1 |
| O(8) | Mn75C025 | 0.4237(1) | 0.2328(2) | 0.3426(2) | 11(1) | 1 |
| | Mn60Co40 | 0.4235(1) | 0.2331(2) | 0.3423(2) | 10(1) | 1 |
| | Mn50Co50 | 0.4237(1) | 0.2334(2) | 0.3421(2) | 11(1) | 1 |
| | Mn40Co60 | 0.4240(1) | 0.2339(1) | 0.3417(1) | 10(1) | 1 |
| O(9) | Mn75C025 | 0.2605(1) | 0.0783(2) | 0.0319(2) | 12(1) | 1 |
| | Mn60Co40 | 0.2604(1) | 0.0784(2) | 0.0318(2) | 13(1) | 1 |
| | Mn50Co50 | 0.2603(2) | 0.0771(2) | 0.0323(2) | 12(1) | 1 |
| | Mn40Co60 | 0.2604(1) | 0.0767(2) | 0.0322(2) | 12(1) | 1 |
| O(10) | Mn75C025 | 0.4205(1) | 0.0070(2) | 0.1538(2) | 21(1) | 1 |
| | Mn60Co40 | 0.4200(1) | 0.0059(2) | 0.1547(2) | 19(1) | 1 |
| | Mn50Co50 | 0.4197(2) | 0.0048(2) | 0.1544(2) | 19(1) | 1 |
| | Mn40Co60 | 0.4192(1) | 0.0046(2) | 0.1543(2) | 18(1) | 1 |

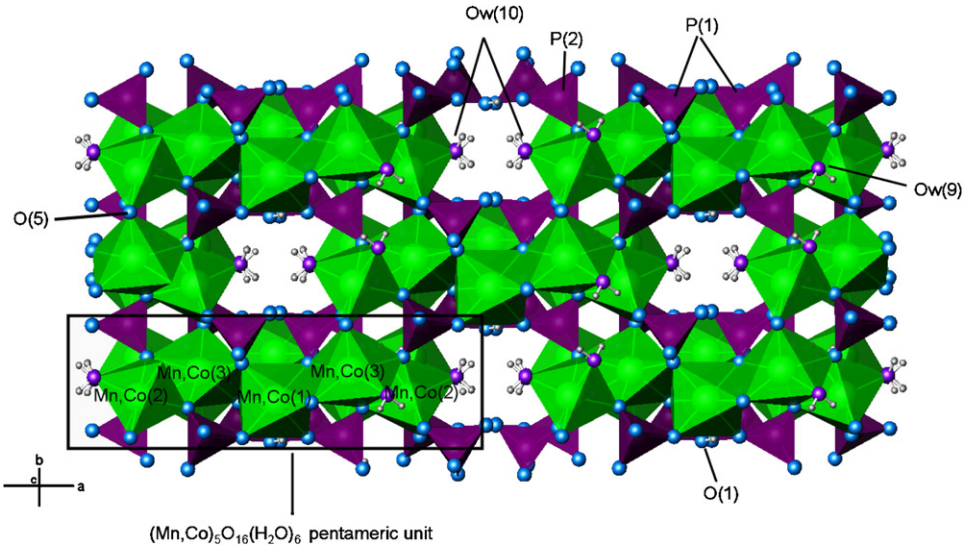


Fig. 2. Polyhedral view of the 3D framework for $Mn_{5-x}Co_x(HPO_4)_2(PO_4)_2 \cdot (H_2O)_4$ ($x = 1.25, 2, 2.5, 3$).

ion in them. As the amount of Co(II) increases, in the four phases, the mean bond distances decrease, according to the minor ionic radius of Co(II) (0.65 Å) in comparison with that of the Mn(II) cation (0.67 Å). Fig. 4 shows the evolution of the mean M–O bond distances with the occupancy factor of Co(II) in each coordination polyhedra.

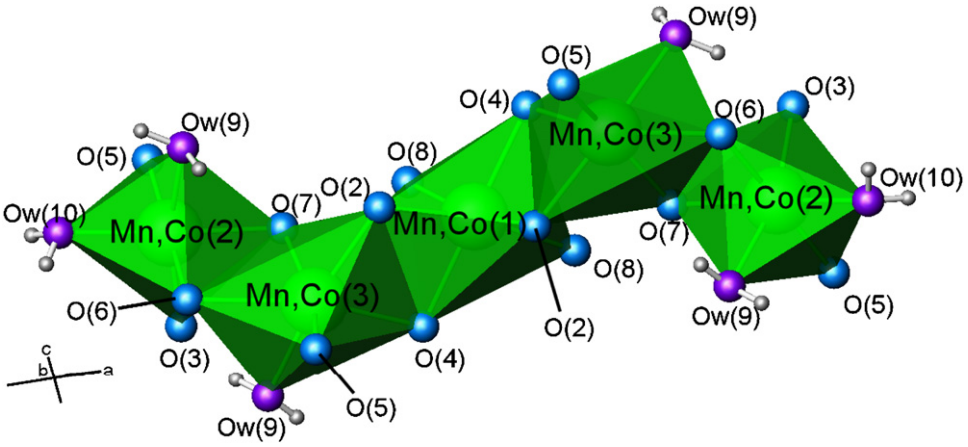


Fig. 3. $(Mn,Co)_5O_{16}(H_2O)_6$ pentameric units of the crystal structure of the $Mn_{5-x}Co_x(HPO_4)_2(PO_4)_2 \cdot (H_2O)_4$ ($x = 1.25$, 2, 2.5, 3) phases.

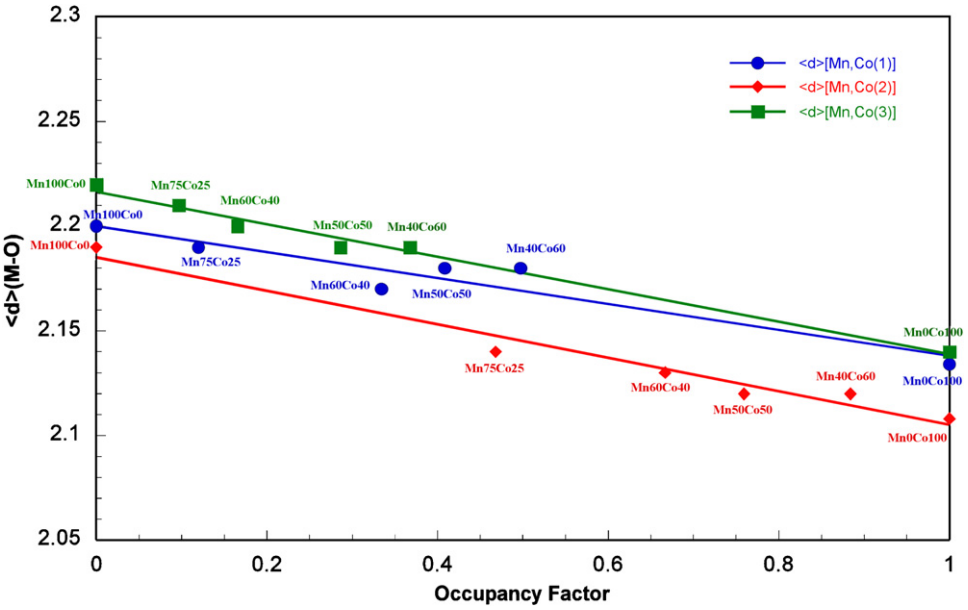


Fig. 4. Mean M–O bond distance evolution as a function of the occupancy factors for Co(II) ions.

The *cis*-bond angles O–MnCo(1)–O, O–MnCo(2)–O and O–MnCo(3)–O range from 70.4(1) to 121.7(1)°. Whereas, the mean *trans*-bond angles have a mean value of 168(7)°.

Taking into account the four phases, in the $P(1)O_4$, hydrogenphosphate and $P(2)O_4$ phosphate tetrahedra the mean P–O bond distances are 1.53(2) and 1.540(8) Å, respectively. The O–P–O bond angles range from 107.51(8)–112.24(8)°.

Distortions of the $[Mn,Co(1)O_6]$, $[Mn,Co(2)O_6]$ and $[Mn,Co(3)O_6]$ polyhedra, from an octahedron ($\Delta = 0$) to a trigonal prism ($\Delta = 1$), have been calculated by the Muetterties and Guggenberger method [21]. It is observed that the distortion of the Mn,Co(1) and Mn,Co(2) polyhedra are smaller in all compounds, approximately, 16% and 13%, respectively, than that obtained for the Mn,Co(3) polyhedra, approximately, 46%.

The unit-cell parameters of this finite solid solution and its volume decrease lineally when the amount of Co(II) cation increases (see Table 1) and it is possible to affirm that the Vegard's law is verified [22].

### 3.2. Infrared and UV–visible spectroscopies

The IR spectra show the bands corresponding to the water molecules, phosphate and hydrogen-phosphate groups [23]. The most important bands of the IR spectra for the four phases studied of the $Mn_{5-x}Co_x(HPO_4)_2(PO_4)_2(H_2O)_4$ ($x = 1.25$, 2, 2.5, 3) finite solid solution are given in Table 3.

In the diffuse reflectance spectra three bands of strong intensity, which increases with increasing the amount in Co(II) cation, are observed. Furthermore, a fourth band is observed, with minor intensity that can be ascribed to a spin forbidden transition of the Mn(II) cation. The spin allowed transitions corresponding to the $d^7$-Co(II) high spin cations have been assigned on the basis of the

Table 3
Seleted IR bands ($cm^{-1}$) for $Mn_{5-x}Co_x(HPO_4)_2(PO_4)_2(H_2O)_4$ ($x = 1{,}25$, 2, 2.5 and 3)

| Group | Bands | Mn75Co25 | Mn60Co40 | Mn50Co50 | Mn40Co60 |
|---|---|---|---|---|---|
| $(PO_4)^{3-}$ | $\nu_{as}$(P–O) | 1150 (w), 1105 (m) | 1150 (w), 1105 (sh) | 1150 (w), 1090 (m) | 1150 (w), 1110 (sh) |
| | | 1070 (s), 1025 (s) | 1070 (s), 1030 (s) | 1060 (s), 1040 (s) | 1070 (s), 1025 (s) |
| | | 980 (sh), 935 (m) | 980 (sh), 935 (m) | 975 (sh), 935 (m) | 980 (sh), 935 (m) |
| | $\nu_s$(P–O) | 760 (w), 710 (w) | 760 (w), 705 (w) | 760 (w), 705 (w) | 760 (w), 715 (w) |
| | $\delta_{as}$(O–P–O) | 580 (m), 525 (m) | 580 (m), 525 (m) | 580 (m), 525 (m) | 580 (m), 525 (m) |
| $(HPO_4)^{2-}$ | δ(P–O–H) | 1315 (w) | 1320 (w) | 1320 (w) | 1330 (w) |
| $H_2O$ | $\nu$(O–H) | 3395 (m) | 3390 (m) | 3390 (m) | 3380 (m) |
| | $\delta$(H–O–H) | 1630 (w) | 1645 (w) | 1650 (w) | 1650 (w) |

s = strong, m = medium, w = weak, sh = shoulder.

Table 4
Assignment (in $cm^{-1}$) of the electronic transitions observed in the diffuse reflectance spectra, and values of the $Dq$ and $B$ ($cm^{-1}$) for the different coordination polyhedra of the four phases of the solid solution

| Assignment | $Co^{2+}$ | $Co^{2+}$ | $Co^{2+}$ | $Mn^{2+}$ |
|---|---|---|---|---|
| | $^4T_{1g}(^4F) \rightarrow {}^4T_{2g}(^4F)$ | $^4T_{1g}(^4F) \rightarrow {}^4A_{2g}(^4F)$ | $^4T_{1g}(^4F) \rightarrow {}^4T_{1g}(^4F)$ | $^6(A_{1g})(^6G) \rightarrow {}^4A_{1g}$, $^4E_g(4G)$ |
| Mn75Co25 | 5610 | 12430 | 17650 | 24660 |
| MnCo(1)Co(2) | 6550 | 14650 | 19300 | |
| MnCo(3) | Mn,Co(1) | Mn,Co(2) | Mn,Co(3) | |
| Dq | 680 | 680 | 810 | |
| *B* | 850 | 850 | 890 | |
| Mn60Co40 | 5650 | 12430 | 17760 | 24650 |
| MnCo(1)Co(2) | 6560 | 14800 | 19230 | |
| MnCo(3) | Mn,Co(1) | Mn,Co(2) | Mn,Co(3) | |
| Dq | 680 | 680 | 820 | |
| *B* | 855 | 855 | 880 | |
| Mn50Co50 | 5660 | 12470 | 17740 | 24650 |
| MnCo(1)Co(2) | 6550 | 14770 | 19300 | |
| MnCo(3) | Mn,Co(1) | Mn,Co(2) | Mn,Co(3) | |
| Dq | 680 | 680 | 820 | |
| *B* | 850 | 850 | 880 | |
| Mn40Co60 | 5700 | 12570 | 17720 | 24630 |
| MnCo(1)Co(2) | 6530 | 14950 | 19320 | |
| MnCo(3) | Mn,Co(1) | Mn,Co(2) | Mn,Co(3) | |
| Dq | 690 | 690 | 840 | |
| *B* | 850 | 850 | 870 | |

Tanabe-Sugano diagrams [24] (see Table 4). These bands show a splitting probably due to the different distortion of the Mn,Co–$O_6$ polyhedra. The Dq and Racah ($B$) parameters have been calculated by using the energy expressions from the Tanabe–Sugano diagrams [25] for a Co(II)-$d^7$ high spin cation in octahedral geometry. The greater value of the Dq parameter has been assigned to the Mn,Co(3)–$O_6$ polyhedron that exhibits the greater octahedral distortion, as can be observed from Table 4.

### 3.3. Magnetic behavior

Magnetic measurements for the $Mn_{5-x}Co_x(HPO_4)_2(PO_4)_2(H_2O)_4$ ($x = 1.25$, 2, 2.5, 3) phases were performed on powdered samples from room temperature to 2.0 K at a magnetic field of 0.1 T. The thermal evolution of the molar magnetic susceptibility, $\chi_m$, and the $\chi_m T$ vs. $T$ product is shown in Fig. 5. The molar magnetic susceptibility, $\chi_m$, of all compounds increases when decreasing temperature and shows maxima at the temperatures given in Table 5. After these maxima the susceptibility decreases slightly (see Fig. 5). The compounds follow the Curie–Weiss law at temperatures higher than 5 K, with values of the Curie and Curie–Weiss temperatures shown in Table 5. The $\chi_m T$ vs. $T$ curve decreases continuously from room temperature to 2.0 K. The continuous decrease of the $\chi_m T$ curve and the negative value of the Curie–Weiss temperature indicate that the major interaction in these compounds are antiferromagnetic and probably three-dimensional in nature taking the structural features into account. These

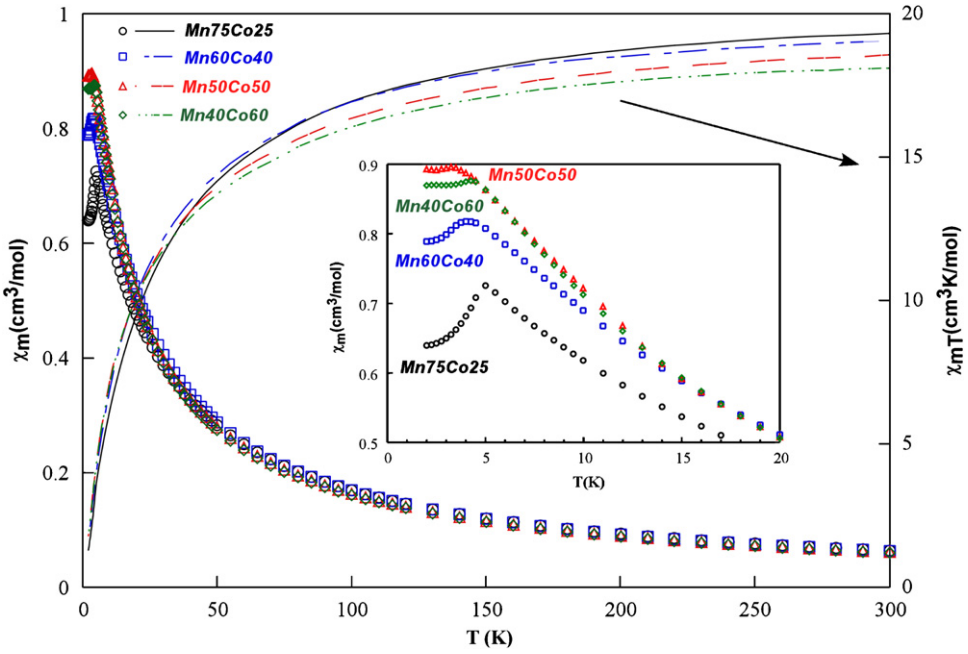


Fig. 5. Thermal evolution of $\chi_m$ and $\chi_m T$ vs. $T$ curves for the $Mn_{5-x}Co_x(HPO_4)_2(PO_4)_2 \cdot (H_2O)_4$ ($x = 1.25$, 2, 2.5, 3) phases.

Table 5
Magnetic data for $Mn_{5-x}Co_x(HPO_4)_2(PO_4)_2(H_2O)_4$ ($x = 1{,}25$, 2, 2.5 and 3) at 1000 Gauss

| Phase | $S'_{HT}$ | $S'_{LT}$ | $T_{max}$ (K) | $(\chi_m)_{max}$ ($cm^3\,mol^{-1}$) | $(\chi_m T)_{max}$ ($cm^3 K\,mol^{-1}$) | $\theta$ (K) | $C_m$ ($cm^3 K\,mol^{-1}$) | $\mu_{eff}$ (BM) |
|---|---|---|---|---|---|---|---|---|
| Mn75Co25 | 2.25 | 2.0 | 5.0 | 0.72 | 3.62 | −23.83 | 20.92 | 12.93 |
| Mn60Co40 | 2.1 | 1.7 | 4.0 | 0.82 | 3.27 | −20.00 | 20.34 | 12.75 |
| Mn50Co50 | 2.0 | 1.5 | 3.5 | 0.89 | 3.13 | −19.82 | 19.76 | 12.57 |
| Mn40Co60 | 1.9 | 1.3 | ≅4.0 | 0.88 | 3.50 | −18.45 | 19.21 | 12.39 |

results are different from those obtained for the isostructural $Mn_5(HPO_4)_2(PO_4)_2 \cdot 4H_2O$ that exhibits a strong ferromagnetic component at 10 K, probably due to a *spin canting* phenomenon [26] of the Mn(II) cations, caused by different orientation of the $Mn(1)O_6$, $Mn(2)$–$O_6$ and $Mn(3)$–$O_6$ sublattices, which are not disposed parallel between them, but establishing an angle with the magnetic field applied (see Fig. 1 of the Supplementary Material). Nevertheless, the Mn(II) and Co(II) mixed cationic compounds do not show a similar phenomenon. In the case of $Co_5(HPO_4)_2(PO_4)_2(H_2O)_4$ antiferromagnetic couplings with a Néel temperature near to 17 K has been evidenced [10].

Both, the value of the effective spin at high temperatures, $S'_{HT}$, taking into account the stoichiometry of the phases, and the value of the effective magnetic moment, $\mu_{eff.}$, have been calculated for the members of the solid solution. The results obtained are given in Table 5. It can be observed that the temperature in the maximum of the magnetic susceptibility, $T_{max.}$, decreases when decreasing the spin effective, $S'_{HT}$, whereas the values of the susceptibility in $T_{max}$ follows the opposite tendency. This first result can be associated with the diminution of the number of non paired electrons when the Mn(II), $d^5$-high spin cation, is changed by the Co(II) one, with a $d^7$-high spin configuration. The value of the related constants to the $\chi_m T$ product, such as, the Curie-constant, $C_m$, and the effective magnetic moment per mol of five magnetic cations, $\mu_{eff.}$, show similar decreasing evolution associated to the decreasing of the effective spin at high temperature, $S'_{HT}$ (see Table 5). The values of the $T_{max.}$ and $(\chi_m T)_{max}$ for the Mn40Co60 phase, with high content in the anisotropic Co(II) cation, do not follow the same decreasing evolution observed for the other three phases. For this phase and also for this one with composition Mn50Co50, irreversibility can be observed in the $\chi_m$ vs. $T$ curve performed in the zero field cooling (ZFC) and field cooling (FC) modes at 0.1 and 0.01 T (Fig. 6). This feature, difficults the exact evaluation of the $T_{max.}$ and that of $(\chi_m T)_{max}$. Nevertheless, for the phases with the higher content in the isotropic Mn(II) cation, Mn75Co25 and Mn60Co40, this effect is not observed. The irreversibility shown by the thermal evolution of the magnetic susceptibility, $\chi_m$, could also be associated with a spin canting phenomenom, or desalinement of the total effective spin at low temperatures, $S'_{LT}$, with respect to a parallel orientation of the octahedra $Mn,Co(1)O_6$, $Mn,Co(2)O_6$ and $Mn,Co(3)O_6$ sublattices, similarly to that proposed for the $Mn_5(HPO_4)_2(PO_4)_2 \cdot$

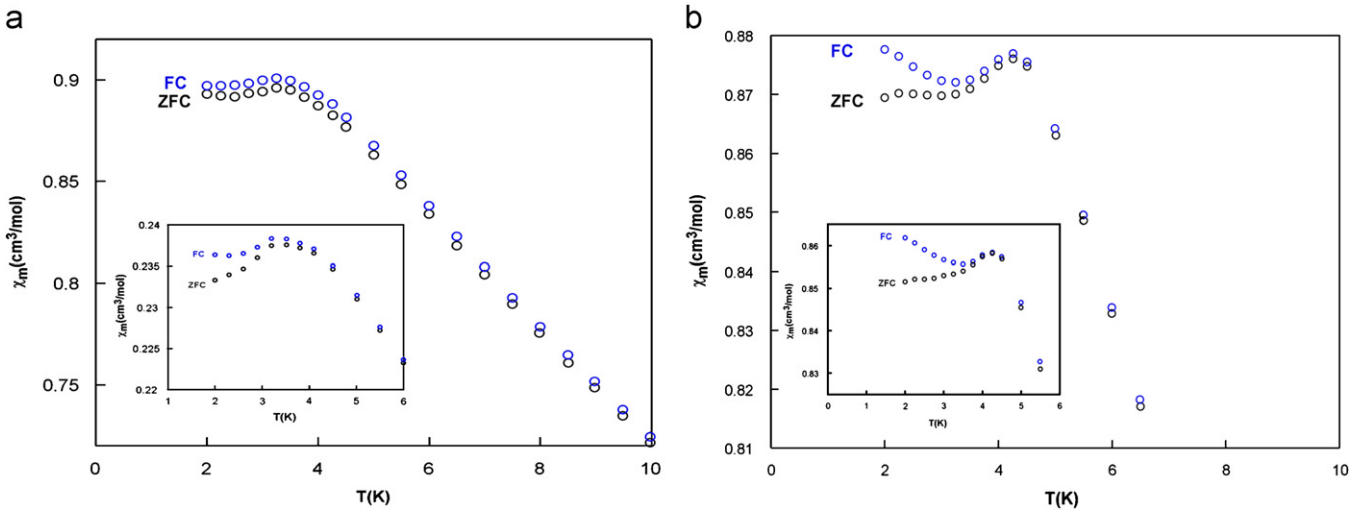


Fig. 6. Thermal evolution at 0.1 T of the ZFC and FC curves for (a) Mn40Co60 and (b) Mn50Co50, showing irreversibility. The insets show the measurements at 0.01 T.

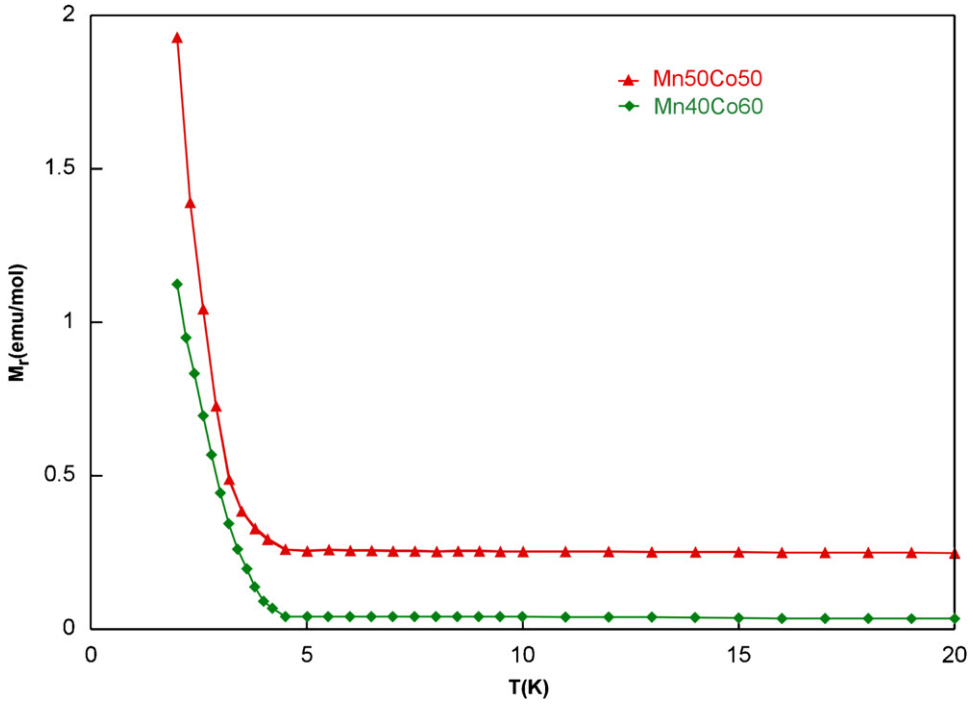


Fig. 7. Thermal evolution of the remnant magnetization curve for Mn50Co50 and Mn40Co60.

$4H_2O$ phase [26]. Additionally, this spin canting phenomenon could be more pronunciated by the characteristic anisotropy of the Co(II) cation [26], because it is not observed for the phases with minor amount in this cation.

In order to corroborate the existence of this weak ferromagnetic component, the thermal evolution of the residual magnetization vs temperature was measured for the Mn50Co50 and Mn40Co60 phases, at 2.0 K under a magnetic field of 0.01 T. The results, shown in Fig. 7, indicate that magnetization disappears at, approximately, 4.5 K. This behavior is characteristic of antiferromagnetic compounds with a weak ferromagnetic component detected at low temperature.

Taking into account the structural features of the $Mn_{5-x}Co_x(HPO_4)_2(PO_4)_2(H_2O)_4$ solid solution a study of the possible magnetic exchange pathways has been performed. The direct magnetic exchange between the metallic centers is not possible because the distance between them is greater than 3.0 Å (see Table 6). Two kinds of superexchange pathways can take place between

Table 6
Intermetallic bond distances (Å) and angles (°) inside the intrapentameric unit for $Mn_{5-x}Co_x(HPO_4)_2(PO_4)_2(H_2O)_4$ ($x = 1{,}25$, 2, 2.5 and 3)

| Distance/angle | Mn75Co25 | Mn60Co40 | Mn50Co50 | Mn40Co60 |
|---|---|---|---|---|
| *d*(*M*2–*M*3) | 3.337(2) | 3.316(2) | 3.310(2) | 3.305(2) |
| *d*(*M*3–*M*1) | 3.347(2) | 3.329(2) | 3.328(2) | 3.324(2) |
| ang(*M*2–*M*3–*M*1) | 115.6(1) | 115.6(1) | 115.5(1) | 115.6(1) |
| ang(*M*3–*M*1–*M*3) | 138.4(1) | 138.5(1) | 138.7(1) | 139.0(1) |

the metallic centers through the oxygen atoms: (i) inside the pentameric entities and (ii) between the pentameric entities. In Fig. 8(a) can be observed that the intrapentameric superexchange pathway takes place through the O(2)–O(4) and O(6)–O(7) edge-sharing of the $MO_6$ octahedra. There are two kinds of interpentameric exchange pathways, along the "*b*" and "*c*" crystallographic axis, respectively (Figs. 8(b) and (c)). Two of them along the "*b*" crystallographic axis, via O(5)-atoms, with the pentameric units disposed in parallel orientation (Fig. 8(b)), an other four along the "*c*" crystallographic axis, via O(9)-atoms, also maintaining a parallel orientation (Fig. 8(c)). In Tables 7 and 8 the bond distances and angles established by the atoms involved in these intra- and inter-pentameric exchange pathways are given. In both superexchange pathways the bond angles have a deviation of, approximately, 10° from the orthogonal angle (90°). This result agrees with the predominance of antiferromagnetic interactions observed in the thermal evolution of the magnetic susceptibility [27]. Additionally, it can be seen (Figs. 8(b) and (c)) that the $MO_6$ sublattices are not placed in parallel orientation with respect to the "*b*" and "*c*" crystallographic axis, but establishing an "α" angle with respect to these crystallographic axes. This fact is probably the origin of the spin canting phenomenon that gives rise to the existence of weak ferromagnetic interactions at low temperatures.

Furthermore, there are super-superexchange pathways in which the phosphate and hydrogenphosphate oxoanions are involved (see Fig. 8). These pathways, propagated via the M–O–P–O–M atoms with bond angles near to 109°, are antiferromagnetic in nature [27].

Finally, it is necessary to indicate that a study by neutron powder diffraction techniques should be performer in order to establish the quantitative values of the magnetic exchange and superexchange pathways and so to know the predominance of the antiferromagnetic couplings above the ferromagnetic ones and vice versa.

## 4. Concluding remarks

$Mn_{5-x}Co_x(HPO_4)_2(PO_4)_2(H_2O)_4$ finite solid solution was synthesized under mild hydrothermal conditions in the form of single-crystals. The structure consists of a three dimensional network formed by octahedral pentameric entities $(Mn,Co)_5O_{16}(H_2O)_6$ sharing vertex with the

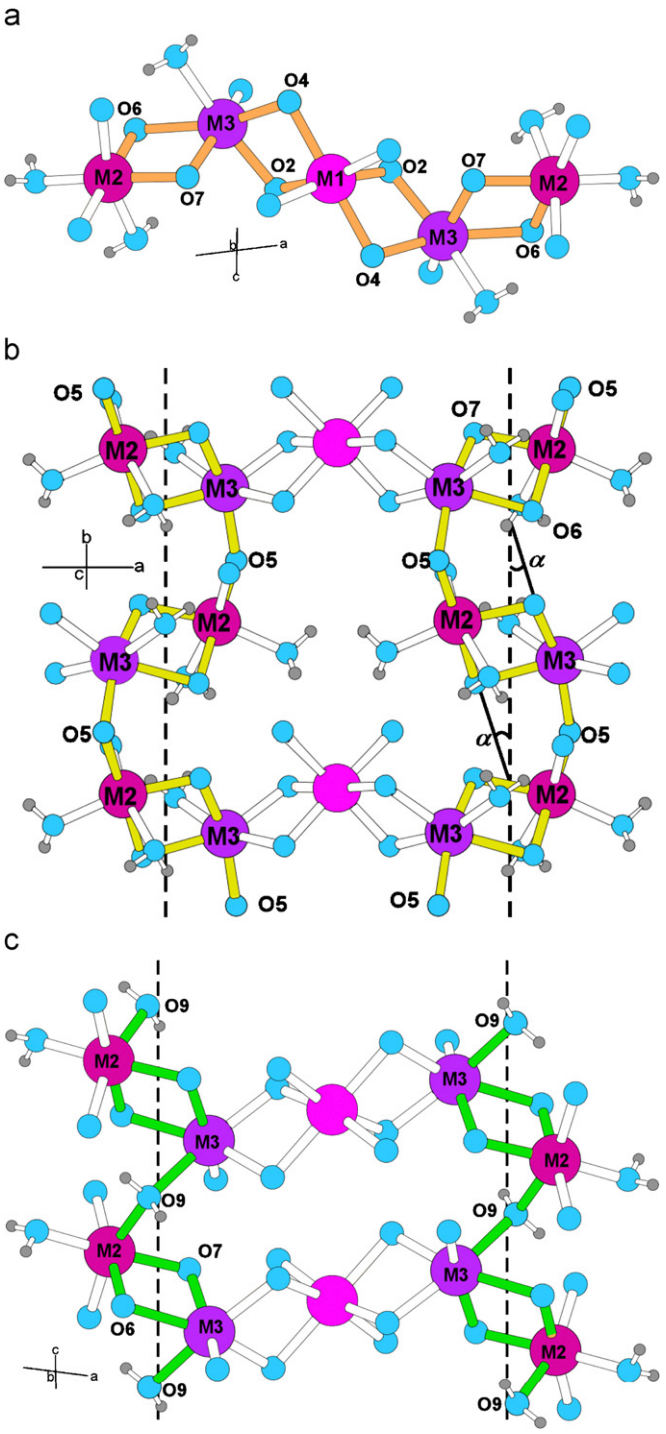


Fig. 8. View of the pentameric unit showing the atoms involved in the magnetic exchange pathways and representation of the α-angle canting with respect to the "*b*" crystallographic axis.

$(PO_4)^{3-}$ and $(HPO_4)^{2-}$ tetrahedra. The three-dimensional network exhibits holes along the [001] direction with the hydrogen atoms of the water molecules pointing out towards them. The IR spectra show the bands of water molecules, the phosphate and hydrogen–phosphate oxoanions. The diffuse reflectance measurements are consistent with slightly distorted octahedral environments for the Mn,$CoO_6$ polyhedra, through the Mn,Co(3)

Table 7
Bond distances (Å) and angles (°) in the intrapentameric units along the "b" crystallographic axis for $Mn_{5-x}Co_x(HPO_4)_2(PO_4)_2(H_2O)_4$ ($x = 1,25$, 2, 2.5 and 3)

| Distance/angle | Mn75Co25 | Mn60Co40 | Mn50Co50 | Mn40Co60 |
|---|---|---|---|---|
| *d*(*M*2–O5) | 2.184(2) | 2.175(2) | 2.178(2) | 2.181(2) |
| *d*(*M*3–O5) | 2.141(2) | 2.131(2) | 2.172(2) | 2.132(2) |
| ang(*M*2–O5–*M*3) | 109.1(1) | 109.3(1) | 109.4(1) | 109.5(1) |

Table 8
Bond distances (Å) and angles (°) in the interpentameric units along the "c" crystallographic axis for $Mn_{5-x}Co_x(HPO_4)_2(PO_4)_2(H_2O)_4$ ($x = 1,25$, 2, 2.5 and 3)

| Distance/angle | Mn75Co25 | Mn60Co40 | Mn50Co50 | Mn40Co60 |
|---|---|---|---|---|
| *d*(*M*2–O9) | 2.241(2) | 2.219(2) | 2.209(2) | 2.203(2) |
| *d*(*M*3–O9) | 2.262(2) | 2.245(2) | 2.239(2) | 2.232(2) |
| ang(*M*2–O9–*M*3) | 111.8(1) | 112.0(1) | 112.6(1) | 112.8(1) |

polyhedron has a higher distortion of 46%. Magnetic measurements indicate the predominance of antiferromagnetic interactions with a spin canting phenomenon detected at low temperatures for the phases with the highest amount in the anisotropic Co(II) cation.

## Acknowledgments

This work was financially supported by the Ministerio de Educación y Ciencia (MAT 2004-02071) and Universidad del País Vasco/EHU (9/UPV00130.310-15967/2004; 9/UPV00169.310-13494/2001) and the "Fondo Europeo de Desarrollo Regional (FEDER), which we gratefully acknowledge. The authors thank the technicians of SGIker, Dr. J. Sangüesa and Dr. I. Orue, financed by the National Program for the Promotion of Human Resources within the National Plan of Scientific Research, Development and Innovation, "Ministerio de Ciencia y Tecnología" and "Fondo Social Europeo" (FSE), for the X-ray diffraction and magnetic measurements, respectively. Edurne S. Larrea thanks to the UPV/EHU for funding.

## Appendix A. Supplementary materials

Supplementary data associated with this article can be found in the online version at doi:10.1016/j.jssc.2007.03.012.

## References

[1] R.C. Haushalter, L.A. Mundi, Chem. Mater. 4 (1992) 31.
[2] A. Clearfield, Chem. Rev. 88 (1988) 125.
[3] F.A. Ruszala, J.B. Anderson, E. Kostiner, Inorg. Chem. 16 (1977) 2417.
[4] P. Vasic, B. Prelesuik, M. Curic, R. Herak, Z. Kristallogr. 173 (1985) 193.
[5] A.R. Kampf, P.B. Moore, Am. Mineral. 61 (1976) 1241.
[6] P.F. Zanazzi, P.B. Leavens, J.S. White, Am. Mineral. 71 (1986) 1244.
[7] P. Lightfoot, A.K. Cheetham, A.W. Sleight, Inorg. Chem. 26 (1987) 3544.
[8] H. Mori, T. Ito, Acta Crystallogr. 3 (1950) 1.
[9] J.M. Rojo, A. Larrañaga, J.L. Mesa, M.K. Urtiaga, J.L. Pizarro, M.I. Arriortua, T. Rojo, J. Solid State Chem. 165 (2002) 171.
[10] (a) Y. Gerault, Y. Riou, Y. Cudennec, Acta Crystallogr. C 43 (1987) 1829;
(b) Z. Han, A. Tian, J. Peng, X. Zhai, J. Solid State Chem. 179 (2006) 2678.
[11] (a) J.M. Rojo, J.L. Mesa, L. Lezama, T. Rojo, J. Mater. Chem. 7 (11) (1977) 2243;
(b) J.M. Rojo, J.L. Mesa, R. Calvo, L. Lezama, R. Olazcuaga, T. Rojo, J. Mater. Chem. 8 (6) (1988) 1423;
(c) J. Escobal, J.L. Mesa, J.L. Pizarro, L. Lezama, R. Olazcuaga, T. Rojo, J. Mater. Chem. 9 (1999) 2691;
(d) J. Escobal, J.L. Pizarro, J.L. Mesa, L. Lezama, R. Olazcuaga, M.I. Arriortua, T. Rojo, Chem. Mater. 12 (2000) 376;
(e) J.M. Rojo, J.L. Mesa, L. Lezama, J. Rodriguez-Fernandez, J.L. Pizarro, M.I. Arriortua, T. Rojo, Int. J. Inorg. Mater. 3 (2001) 67;
(f) E. Alda, S. Fernandez, J.L. Mesa, J.L. Pizarro, V. Jubera, T. Rojo, Mater. Res. Bull. 37 (2002) 2355;
(g) J. Escobal, J.L. Pizarro, J.L. Mesa, J.M. Rojo, B. Bazan, M.I. Arriortua, T. Rojo, J. Solid State Chem. 178 (2005) 2626;
(h) A. Goñi, J.L. Mesa, J.L. Pizarro, L. Fournes, A. Wattiaux, R. Olazcuaga, M.I. Arriortua, T. Rojo, J. Solid State Chem. 179 (2006) 81.
[12] J.L. Pizarro, G. Villeneuve, P. Hagenmuller, A. Le Bail, J. Solid State Chem. 92 (2) (1991) 273.
[13] A. Boultif, D.J. Louër, Appl. Crystallogr. 24 (1991) 987.
[14] Rodríguez-Carvajal. FULLPROF98, Program for Rietveld Pattern Matching Analysis of Powder Patterns, Grenoble, 1998, unpublished.
[15] (a) Powder Diffraction File—Inorganic and Organic, ICCD Files 29–0891;
(b) Powder Diffraction File—Inorganic and Organic, ICCD Files 39–0709;
(c) Powder Diffraction File—Inorganic and Organic, ICCD Files 40–0102.
[16] Oxford Diffraction Ltd., CRYSALIS, version 1.170.32, 2003.
[17] G.M. Sheldrick, SHELXS97: Program for the Refinement of Crystal Structures, University of Göttingen, Germany, 1997.
[18] G.M. Sheldrick, SHELXL97: Program for the Solution of Crystal Structures, University of Göttingen, Germany, 1997.
[19] International Tables for X-ray Crystallography, vol. VI, KYnoch Press, Birmingham, England, 1974, p. 99.
[20] E. Dowty, ATOMS: A Computer Program for Displaying Atomic Structures, Shape Software, Kingsport, TN, 1993.
[21] E.L. Muetterties, L.J. Guggenberger, J. Am. Chem. Soc. 96 (1974) 1748.
[22] A.R. West, Basic Solid State Chemistry, Wiley, Chichester, West Sussex, 1988.
[23] K. Nakamoto, Infrared and Raman Spectra of Inorganic and Coordination Compounds, Wiley, New York, 1997.
[24] Y. Tanabe, S.J. Sugano, Phys. Soc. Japan 9 (1954) 753.
[25] A.B.P. Lever, Inorganic Electronic Spectroscopy, Elsevier Science Publishers B.V., Amsterdam, Netherlands, 1984.
[26] R.L. Carlin, Magnetochemistry, Springer, Berlin, Heidelberg, 1986.
[27] J.B. Goodenough, Magnetism and Chemical Bond, Interscience, New York, 1963.